Progress In Electromagnetics Research C, Vol. 136, 113–121, 2023

Design of Ultra-Miniaturized Wearable Antenna for Bio-Telemetry Applications

Regalla Narendra Reddy[1, *], Nalam V. Koteswara Rao[2], Dasari Rama Krishna[1], and Jeet Ghosh[2]

Abstract—In this paper, an ultra-miniaturized, planar dual-band wearable antenna is proposed for bio-telemetry applications. The proposed antenna covers the 433 MHz and 915 MHz Industrial, Scientific, and Medical (ISM) bands with a compact volume of $0.000000384\lambda_0^3$. The antenna consists of a meander line on the top side of the substrate, while the backside is loaded with an inductive grid structure to achieve miniaturization. Moreover, the absence of vias in the design of the antenna offers a significant benefit in terms of simplifying the fabrication process. The design approach considers the integration of other components for device-level architecture. The antenna exhibits stable performance when being placed on different human body parts, such as the head and hand. The evaluated specific absorption rate (SAR) complies with the regulated human safety standard. Additionally, the link margin (LM) calculation shows that the antenna could establish a biotelemetry communication link at a distance of 20 meters.

1. INTRODUCTION

The emerging technology of wearable electronics is offering numerous healthcare applications such as endoscopy, neural recording, and glucose monitoring. A conventional wearable telemetry device is made up of one body control unit (BCU) and one or more body sensor units (BSUs) [1]. BCU can receive physiological signal data from BSUs and transmit it to a remote access point. To be able to maintain an effective communication link to the external unit, an efficient wearable antenna plays an important role in wearable devices. For maintaining the compactness and comfortability of the wearable devices, the antenna should be very small, low profile, and mechanically strong [2].

In the literature, several wearable antennas have been reported for wireless body area network (WBAN) applications at different Industrial, Scientific, and Medical (ISM) frequency bands, such as 0.433/0.915/2.45/5.85 GHz. In general, the footprint of the antenna is relatively small in the high-frequency region. For this reason, researchers are keen to design numerous wearable antennas at 2.45/5.85 GHz using a variety of geometries, including rectangular patches [3], circular patches [4], meander bowtie antennas [5], and co-planar waveguide (CPW)-fed monopoles [6]. A wearable antenna integrated with defected ground structure (DGS) and neutralization line (NL) has been presented in [7]. It should be mentioned that the high-frequency regions are prone to attenuation and propagation loss [8]. In this regard, the 433 MHz and 915 MHz frequency bands also have importance for the design of wearable antennas. The main design problem for low-frequency antennas is their size. In [9], an antenna unit with a volume of 1267.2 mm^3 is proposed for the communication in 400 MHz frequency band. Likewise, an alternate solution based on a meanderline monopole antenna is presented in [10]. It is observed that the antenna covers a large area of dimensions ($0.085\lambda_0 \times 0.075\lambda \times 0.002\lambda$) in wearable

Received 26 June 2023, Accepted 1 August 2023, Scheduled 14 August 2023

* Corresponding author: Regalla Narendra Reddy (narendra.r@uceou.edu).

[1] ECE Department, University College of Engineering, Osmania University, Hyderabad, Telengana, India. [2] ECE Department, Chaitanya Bharathi Institute of Technology, Hyderabad, Telangana, India.

devices. To miniaturize the size of the antenna, various miniaturization techniques, such as vias and slots, have been reported in [11]. However, the excessive use of via increases the design complexity and electrical losses. Furthermore, to establish a reliable and sensible link, multiband antennas are gaining huge interest in the wearable industry. A wearable multiband monopole antenna has been proposed [12] with a significant footprint. Because of the significant dimensions of the antenna, this design is not ideal for wearable devices. To miniaturize the size of the antenna, a folded geometry-based structure is presented in [13]. However, the folded geometry increases the lateral height of the antenna. A compact dual-band multilayer folded-cavity antenna loaded with lumped elements has been developed [14]. Due to the lumped elements and multilayer structure, the antenna may not be suitable for the wearable application. A multi-band dipole antenna integrated with an inductively coupled meander shape has been proposed in [15]. It has been noticed that the proposed wearable antenna has an overall dimension of $60 \times 40 \times 0.254\,\text{mm}^3$. Recently, the structure established in [16] has been used to minimize antenna size by etching Moore's fractal geometry into a rectangular patch and then extending it over a rectangle loop with a defective ground structure. It is observed from the literature that most of the reported antennas have a significant dimension, which reduces the comfortability of the wearer and increases the dimension of the wearable devices.

In this work, an ultra-miniaturized dual-band wearable antenna operating in the 433 MHz and 915 MHz bands is designed for WBAN applications. This antenna is fed using a CPW structure and fabricated on an FR4 substrate (permittivity = 4.4). The design process starts with the miniaturization of the monopole antenna using a meandering technique. In an effort to further miniaturize the antenna, an inductive grid pattern has been etched out beneath the patch on the bottom surface. It is relatively small, with a dimension of 22 mm × 21 mm, and relatively thin, with a thickness of 0.3 mm. The simulated and measured results were compared and presented. A study on specific absorption rate (SAR) for patient safety is conducted, and the impact of embedded components on practical usage of the device has also been evaluated. In addition, the link margin (LM) study of the antenna is assessed to look into its compatibility for bio-telemetry communication.

2. ANTENNA TOPOLOGY AND DESIGN

The geometry of the proposed ultra miniaturized co-planar waveguide-fed meander line antenna (CPW-MA) is exhibited in Figure 1. A thin substrate is chosen to enhance wearer's comfort and ease of integration with the wearable devices. The antenna is composed of a meandered monopole and a planar inductive grid on the top and bottom sides of the substrate, respectively. The total dimension of the antenna is 22 mm × 21 mm, and the optimized parameters of the proposed antenna are enlisted in Table 1.

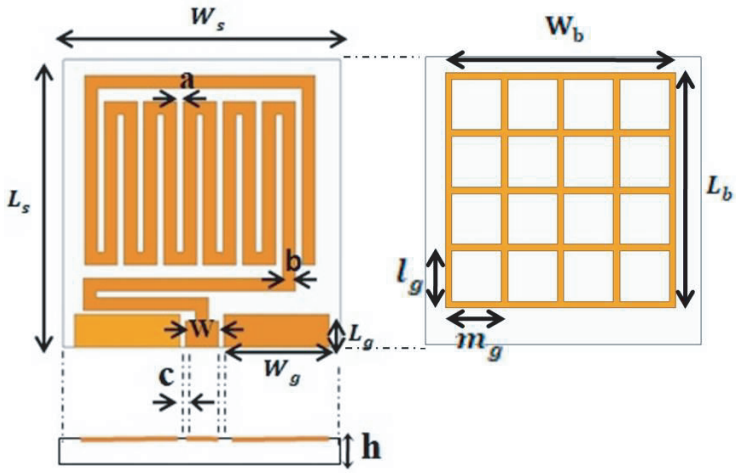

Figure 1. Geometry of the proposed antenna.

Table 1. Geometrical parameters of the proposed antenna.

Parameter	L_s	W_s	L_g	W_g	L_b	W_b	W
Dimensions (mm)	22	21	2.5	8	18	17.6	2.5
Parameter	l_g	m_g	a	b	c	h	
Dimensions (mm)	4.4	4.5	0.5	1	0.4	0.3	

2.1. Evolution Process of CPW-MA

In the following section, a step-by-step development of the CPW-MA is presented. Figure 2 illustrates the structural development of the miniaturized CPW-MA and its associated reflection coefficient. Primarily, a ring-shaped monopole antenna is considered and presented as stage 1 in Figure 2(a). From Figure 2(b), it is observed that the antenna in stage 1 resonates at a 1.30 GHz frequency. In addition, the input impedance of the antenna is also monitored and exhibited in Figure 2(c). It is observed from this figure that at the lower frequency, the antenna in stage 1 provides the capacitive impedance. In order to reduce the capacitive reactance of the structure, a meandering line configuration is incorporated into the structure and mentioned as stage 2. The effective capacitance has been lowered because of the inductive reactance offered by the arms of the meandering structure. However, because of the open-ended transmission line, a significant amount of capacitance continues to exist at the lower frequency, as exhibited in Figure 2(c). In stages 1 and 2, the back surface of the substrate is completely etched to remove the metal. Furthermore, for the purpose of reducing the capacitive reactance at the required frequency of 433 MHz, an inductive grid structure is loaded onto the back side of the substrate at stage 3.

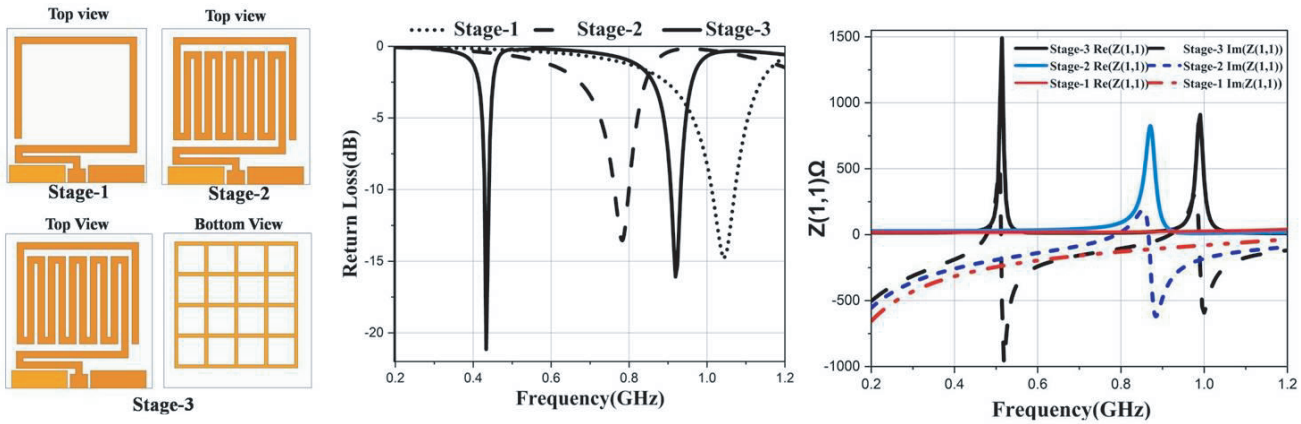

(a) (b) (c)

Figure 2. (a) Developmental stages of proposed design. (b) Return Loss plot from stage 1 to stage 3. (c) Impedance plot from stage 3 to stage 1.

As a result of the inductance provided by the loaded grid structure, there is a significant reduction in the capacitive reactance of the resultant antenna. Furthermore, the antenna exhibits an impedance match at the required ISM frequency band of 433 MHz, as shown in Figure 2(c). In addition to the fundamental resonating frequency of 433 MHz, the antenna also exhibits an impedance match in the 915 MHz frequency band. To understand the electromagnetic behaviour of our proposed structure, we monitored the electric field distribution of each stage at 433 MHz inside the dielectric layer and plotted it in Figure 3. It is well known that the accumulation of a strong electric field inside the dielectric indicates the capacitive behaviour of the substrate. It is noticed from Figure 3 that a strong electric field is observed inside the dielectric layer around the metallic structure in stage 1. Thus, the ring shaped monopole antenna has capacitive behaviour in the lower frequency region.

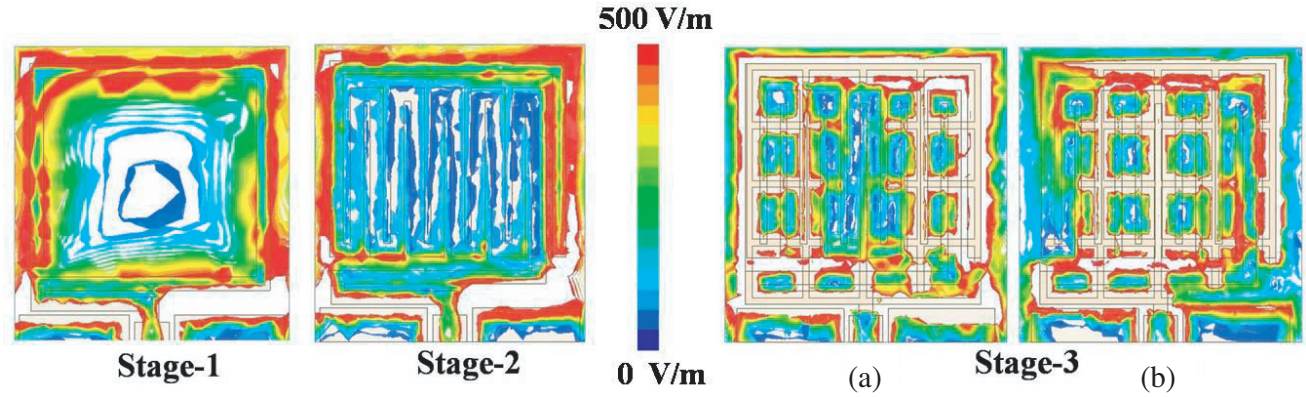

Figure 3. Magnitude E-field distribution of stage 1, stage 2 and stage 3 (a) at 433 MHz, stage-3 (b) at 915 MHz.

To reduce the capacitance, a meanderline-based structure is included in the antenna geometry in stage 2. Due to the meanderline, the inductance of the structure increases, which reduces the capacitive behaviour. As a result, less electric field is accumulated in stage 2 than in stage 1. However, around the open-ended transmission line, a significant electric field is also noticed.

In the final stage, after loading the inductive grid, the accumulation of electric fields is significantly reduced, as exhibited in Figure 3. We also monitored the surface current distribution of the proposed antenna at resonating frequencies of 433 MHz and 915 MHz, as exhibited in Figures 4(a) and (b), respectively. A noticeable amount of surface current is observed around the meander line and inductive grid. This phenomenon indicates that the aforementioned regions provide strong inductance in the structure.

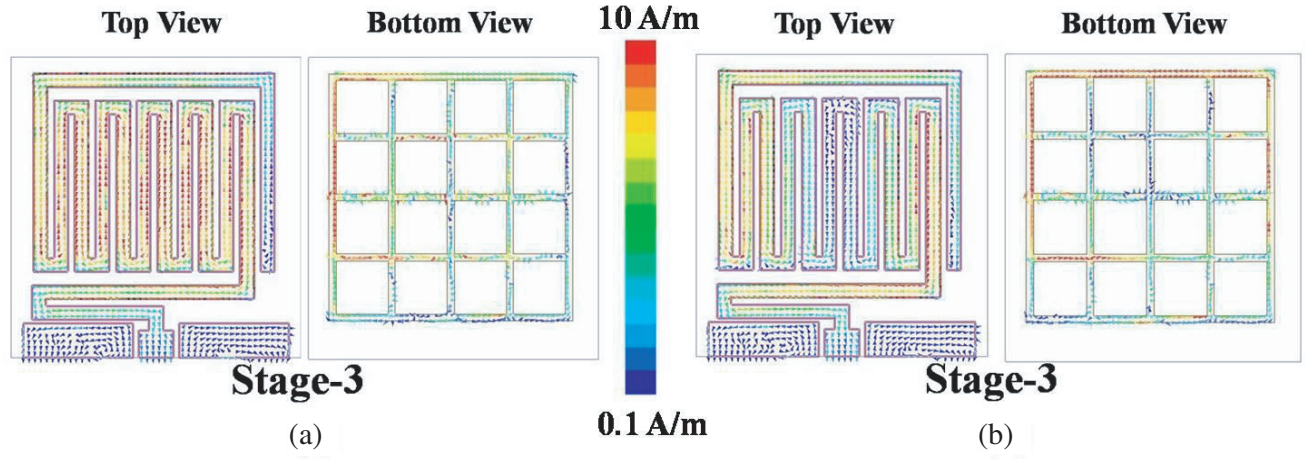

Figure 4. Surface Current distribution of Stage 3 (a) at 433 MHz and (b) at 915 MHz.

2.2. Antenna Testing and Measured Results

To confirm the performance of the suggested antenna design under realistic conditions, a physical prototype was created and tested. The prototype was subjected to return loss measurement using an "Anritsu S820E Site Master Handheld Cable & Antenna Analyzer". The results were then compared to the simulated data. The measured return loss, displayed in Figure 5(c), reveals that the fabricated prototype operates at two frequencies, namely 433 MHz and 915 MHz, in free space. The radiation performance of the antenna at the specified operating frequencies in the E- and H-planes was also

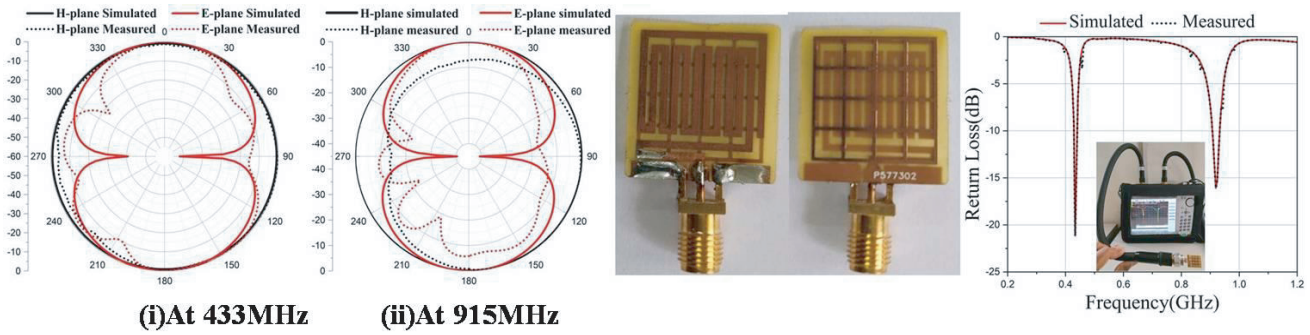

Figure 5. Measured radiation patterns of antenna in free space, (a) E-plane and H-plane, (i) at 433 MHz, (ii) at 915 MHz, (b) fabricated prototype, (c) measured and simulated return loss.

investigated. The simulated radiation pattern at 433 MHz and 915 MHz is presented in Figure 5(a). To verify the accuracy of the simulations, the antenna's radiation pattern was measured inside an anechoic chamber. The measured results were then compared to the simulated ones in Figure 5(a).

The comparison demonstrated a strong agreement between the two, confirming the validity of the simulated data. In addition, the experimental results indicate that the proposed antenna has maximum peak gains of 0 dBi and −15.90 dBi, at 433 MHz and 915 MHz, respectively. The fabricated prototype is exhibited in Figure 5(b). In conclusion, the antenna prototype was fabricated and tested through return loss and radiation pattern measurements. The measured results aligned well with the simulated ones, validating the performance of the fabricated antenna.

3. EFFECTS OF HUMAN BODY PROXIMITY ON ANTENNA PERFORMANCE

To assess the impact of changes in the electrical properties of different human body parts on antenna performance, the researchers conducted experiments with the antenna positioned at various locations, as depicted in Figure 6. Figure 6(a) presents a comparison of the proposed antenna's performance on the human body at two distinct positions (head and hand) by measuring the reflection coefficients in free space across the operating frequency range. The measured and simulated return losses demonstrate excellent agreement, indicating consistent characteristics in terms of return losses. As the prototype

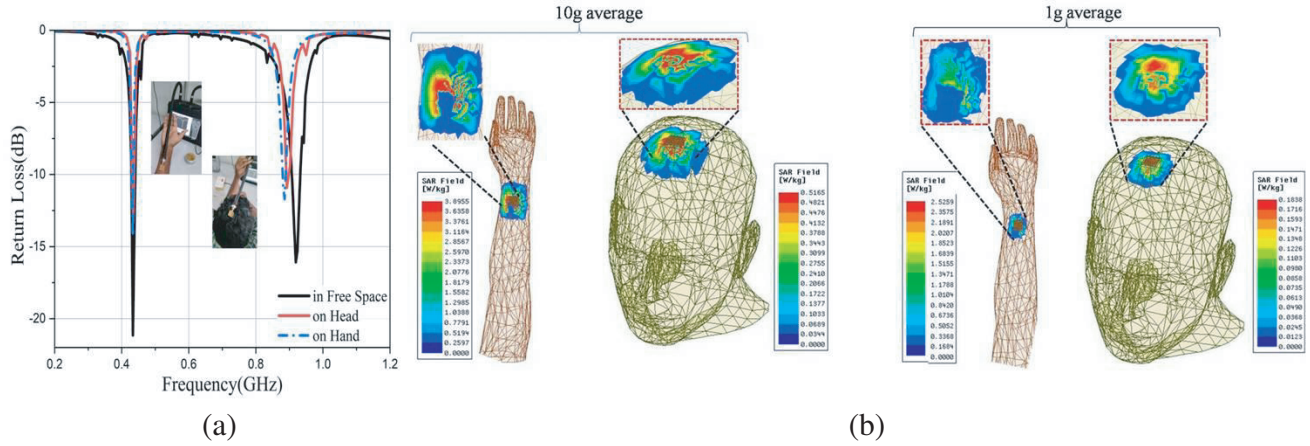

Figure 6. Assessment of Antenna SAR using a human body model. (a) Comparative analysis of return loss: Free space vs. hand and head positions. (b) Three-dimensional SAR distribution of antenna at 433 MHz on hand and head position.

antenna is moved to different locations (head and hand), the reflection coefficient experiences slight changes, suggesting a slight downward shift in the frequency range of the second resonating band due to detuning effects caused by the presence of the human body. The antenna is designed to cover the frequency bands exclusively reserved for bio-telemetry communication and has been thoroughly evaluated under both free space and on-body conditions. This evaluation enables a comprehensive understanding of the antenna's performance in realistic on-body scenarios, facilitating the design of antennas suitable for bio-telemetry applications.

3.1. SAR Evaluation and Link Budget Analysis

To meet the safety criteria for wearable applications, the proposed antenna must comply with Specific Absorption Rate (SAR) limits. The SAR regulations outlined by the IEEE standard [17, 18] restrict the average SAR over 1 gram of tissue to below 1.6 W/kg and over 10 grams of tissue to below 2 W/kg. For the sake of brevity, this study focuses on SAR values for 1 gram of tissue. Figure 6(b) illustrates the evaluation and comparison of SAR performance for antennas on human body models, specifically considering the maximum input power at the arm and head positions with respect to the defined safety criteria.

Simulated SAR values for the proposed antenna on the arm model are 2.53 W/kg for 1 gram of tissue and 3.89 W/kg for 10 grams of tissue, using an input power of 1 W. To satisfy the SAR requirements, the maximum allowable input power is determined as 0.63 W for 1 gram of tissue and 0.55 W for 10 grams of tissue. Table 2 provides a summary of the maximum permissible input power for the proposed antenna at different positions, ensuring compliance with established health and safety standards. The findings indicate that the maximum allowable input power is 0.63 W at the arm position, while the lowest permissible input power is 0.2 W at the head position, in accordance with IEEE safety regulations. This study demonstrates that the proposed antenna can operate within the specified IEEE SAR limits. The maximum input power of 0.63 W is acceptable at the arm position, while the lowest acceptable input power is 0.2 W at the head position, ensuring compliance with safety requirements.

Table 2. Compliance with SAR limits: Maximum values for antenna positions on human body models.

Antenna position	**1 g Tissue [W/kg]/ Input Power [W]**	**10 g Tissue [W/kg]/ Input Power [W]**
On Arm	0.63	0.55
On Head	0.20	0.51

The link budget analysis evaluates the communication capabilities of a proposed antenna compared to an external standard dipole antenna with a gain of 2.15 dB placed at a distance 'd' in open space. The link margin (LM) for far-field wireless communication is calculated using the Friis Transmission Formula [19], which can be expressed as follows:

$$\begin{aligned} \textit{Link Margin}\,(\text{dB}) &= \textit{Link}\ \frac{C}{N_0} - \textit{Required}\ \frac{C}{N_0} \\ &= P_t + G_t - L_f + G_r - N_0 - \frac{E_b}{N_0} + 10\log_{10} B_r + G_c - G_d \end{aligned}$$

where $L_f\,(\text{dB}) = 20\log_{10}\frac{4\pi d}{\lambda}$.

The receiver gain, denoted as G_r, is assumed to be 2.15 dBi for a standard dipole antenna, according to [20]. The path loss is represented by L_f; P_t signifies the input power; N_0 represents the noise power; and B_r indicates the bit rate. However, the transmitter gains (G_t) and resonance frequency deviate from the values specified in [19]. The link margin for the suggested antenna is calculated at 433 MHz and 915 MHz ISM bands, considering bit rates of 100 kbps and 7 Mbps, as shown in Figure 7(a). The results demonstrate that, with the supplied power levels of −10 dBm across the operational frequency bands, the link margin surpasses 20 dB at a distance of 20 meters.

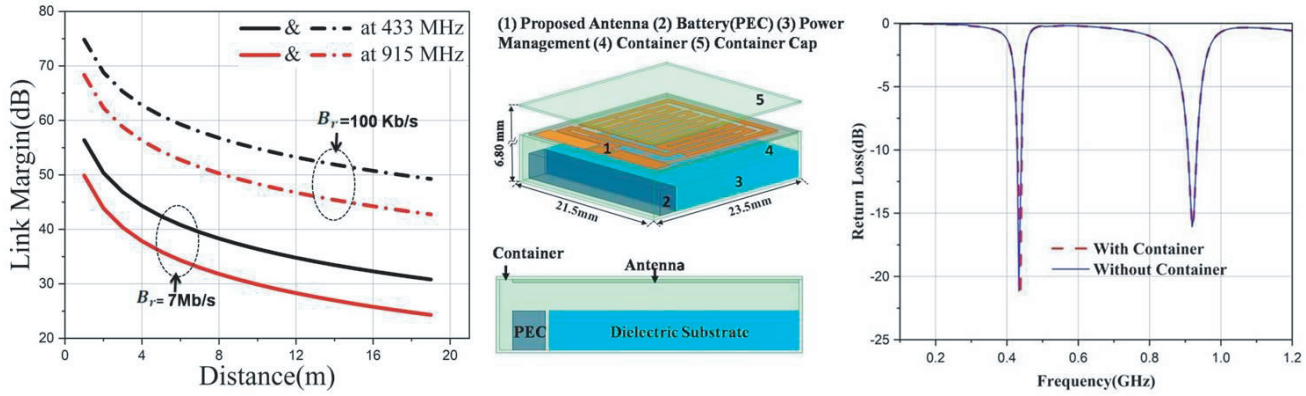

(a) (b) (c)

Figure 7. (a) Link margin. (b) An expansive outlook of the wearable system. (c) Return loss of the proposed antenna.

3.2. Antenna Placement Analysis

To enable the transmission of biomedical information through wearable devices, it is necessary to include extra components along with the antenna. The evaluation of the device is performed by integrating the antenna with additional electronic hardware within a biocompatible ceramic alumina enclosure that is 0.25 mm thick and has a permittivity of 9.8. Figure 7(b) provides an expansive view of the wearable device, while Figure 7(c) illustrates the simulated S-parameter of the proposed antenna. It is observed that the antenna, when being integrated with the additional components, exhibits slightly less deviation from its isolated state, implying that the performance of the antenna is relatively unaffected by their inclusion. This evaluation process ensures that the wearable device effectively communicates biomedical information while maintaining biocompatibility and optimal antenna performance.

3.3. Comparative Assessment of Antenna Performance Metrics

The provided information in Table 3 outlines the comparison between the proposed antenna and the existing state-of-the-art dual-band wearable antennas discussed in the literature. With respect to the size listed in Table 3, it is evident that the suggested antenna has a small footprint.

Table 3. Proposed wearable antenna with respect to other dual-band antennas.

Ref.	Overall Size (λ_0^3) ($L \times W \times h$)	Resonant Frequency
[8]	$0.264\times0.05\times0.002 = 2640 \times 10^{-8}$	400 MHz
[9]	$0.085 \times 0.075 \times 0.002 = 1275 \times 10^{-8}$	433 MHz
[10]	$0.08\times0.08\times0.006 = 3840 \times 10^{-8}$	915 MHz
[13]	$0.03\times0.03 \times 0.007 = 630 \times 10^{-8}$	433/915 MHz
Proposed Antenna	$0.03\times0.03 \times 0.0004 = 36 \times 10^{-8}$	433/915 MHz

4. CONCLUSION

A compact, dual-band wearable antenna designed for bio-telemetry applications at 433/915 MHz frequencies has been successfully demonstrated. The size of the antenna is very small, measuring $0.032\lambda_0 \times 0.030\lambda_0 \times 0.0004\lambda_0$. The via-free configuration is also a beneficial characteristic of this work in terms of fabrication difficulty, with a significant reduction in physical size. Measurements conducted in

free space and on the human body confirm that the SAR values of the antenna at both frequencies meet the regulated human safety standard. Additionally, the return loss and measured radiation patterns in an anechoic chamber room closely match the simulated results, validating the antenna's suitability for on-body bio-telemetry applications.

REFERENCES

1. Hall, P. S. and Y. Hao, *Antennas and Propagation for Body-centric Wireless Communications*, Artech House, Norwood, MA, USA, 2012.
2. Fang. G., E. Dutkiewicz, M. A. Huq, R. Vesilo, and Y. Yang, "Medical body area networks: Opportunities, challenges and practices," *Proc. 11th Int. Symp. Commun. Inf. Technol.*, 562–567, 2011.
3. Zhu, S. and R. Langley, "Dual-band wearable textile antenna on an EBG substrate," *IEEE Trans. Antennas Propag.*, Vol. 57, No. 4, 926–935, Apr. 2009.
4. Liu, Z. G. and Y. X. Guo, "Dual band low profile antenna for body centric communications," *IEEE Trans. Antennas Propag.*, Vol. 61, No. 4, 2282–2285, Apr. 2013.
5. Othman, N., N. A. Samsuri, M. K. A. Rahim, and K. Kamardin, "Low specific absorption rate and gain-enhanced meandered bowtie antenna utilizing flexible dipole-like artificial magnetic conductor for medical application at 2.4 GHz," *Microw. Opt. Technol. Lett.*, Vol. 62, 3881–3889, 2020.
6. Mersani, A., L. Osman, and J.-M. Ribero, "Performance of dual-band AMC antenna for wireless local area network applications," *Microw., Antennas Propag.*, Vol. 12, No. 6, 872–878, May 2018.
7. Biswas, A. K. and U. Chakraborty, "Investigation on decoupling of wide band wearable multiple-input multiple-output antenna elements using microstrip neutralization line," *Int. J. RF Microw. Comput. Aided Eng.*, Vol. 29, e21723, 2019.
8. Gemio, J., et al., "Human body effects on implantable antennas for ISM bands applications: Models comparison and propagation losses study," *Progress In Electromagnetics Research*, Vol. 110, 437–452, 2010.
9. Sabban, A., "Small wearable antennas for wireless communication and medical systems," *2018 IEEE Radio and Wireless Symposium (RWS)*, 161–164, Anaheim, CA, USA, 2018.
10. Suzan Miah, M., A. N. Khan, C. Icheln, K. Haneda, and K.-I. Takizawa, "Antenna system design for improved wireless capsule endoscope links at 433 MHz," *IEEE Trans. Antennas Propag.*, Vol. 67, No. 4, 2687–2699, Apr. 2019.
11. Mohamed, A. E., A. H. Muqaibel, and M. S. Sharawi, "Superstrate loaded miniaturized patch for biomedical telemetry," *Microw. Opt. Technol. Lett.*, Vol. 59, 1212–1218, 2017.
12. Michalopoulou A., A. Alexandridis, T. Zervos, and F. Lazarakis, "A wearable multiband monopole antenna for digital television and wireless communications," *The 8th European Conference on Antennas and Propagation (EuCAP 2014)*, 1398–1402, The Hague, Netherlands, 2014.
13. Rezaeieh, S. A. and A. M. Abbosh, "Wideband and unidirectional folded antenna for heart failure detection system," *IEEE Antennas Wireless Propag. Lett.*, Vol. 13, 844–847, 2014.
14. Zhang, H., X. Chen, M. Li, F. Yang, and S. Xu, "A compact dual-band folded-cavity antenna for microwave biomedical imaging applications," *Proc. IEEE Int. Conf. Comput. Electromagn.*, 1–3, Mar. 2019.
15. Dey, A., D. Mitra, and W. Arif,, "Design of CPW fed multiband antenna for wearable wireless body area network applications," *International Journal of RF and Microwave Computer-Aided Engineering*, 2020.
16. Khan, U. R., J. A. Sheikh, A. Junaid, R. Amin, S. Ashraf, and S. Ahmed, "Design of a compact hybrid Moore's fractal inspired wearable antenna for IoT enabled bio-telemetry in diagnostic health monitoring system," *IEEE Access*, Vol. 10, 116129–116140, 2022.
17. IEEE Standard for Safety Levels with Respect to Human Exposure to Radio Frequency Electromagnetic Fields, 3 kHz to 300 GHz. *IEEE Std C95.1-1999*. 1999.

18. IEEE Standard for Safety Levels with Respect to Human Exposure to Radio Frequency Electromagnetic Fields, 3 kHz to 300 GHz. (*Revision of IEEE Std C95.1-1991*), 2006.
19. Xia, W., K. Saito, M. Takahashi, and K. Ito, "Performances of an implanted cavity slot antenna embedded in the human arm," *IEEE Trans. Antennas Propag.*, Vol. 57, No. 4, 894–899, 2009.
20. Fan, Y., J. Huang, T. Chang, and X. Liu, "A miniaturized four-element MIMO antenna with EBG for implantable medical devices," *IEEE Journal of Electromagnetics, RF and Microwaves in Medicine and Biology*, Vol. 2, No. 4, 226–233, Dec. 2018.